References

AUTHIER, A. (1966). *Advanc. X-ray Anal.* **10**, 9.
BONSE, U. (1964). *Z. Physik*, **177**, 543.
BORRMANN, G., HARTWIG, W. & IRMLER, H. (1958). *Z. Naturforschg.* **13a**, 423.
International Tables for X-ray Crystallography (1962). Vol. III, p. 237. Birmingham:Kynoch Press.
KAMBE, K. (1963). *Z. Naturforsch.* **18a**, 1010.
KATO, N. (1958). *Acta Cryst*, **11**, 885.
KATO, N. (1960). *Acta Cryst.* **13**, 349.
LANG, A. R. (1959). *Acta Cryst.* **12**, 249.
LAUE. M. VON (1960). *Röntgenstrahlinterferenzen.* Frankfurt am Main: Akademische Verlagsgesellschaft.
MEIER, F. (1962). *Z. Physik*, **168**, 10.
YONG, F. W., BALDWIN, T. O., MERLINI, A. E. & SHERRILL, F. A. (1965). *Advanc. X-ray Anal.* **9**, 1.

Acta Cryst. (1971). A**27**, 22

Diffraction Intensities from a Cluster of Curved Crystallites. III. The Three-Dimensional Case

BY G. B. MITRA AND S. BHATTACHERJEE

Department of Physics, Indian Institute of Technology, Kharagpur, India

(*Received* 24 *September* 1969)

A general expression for the intensity of X-rays diffracted by a conglomeration of identical cylindrical crystallites with a given angular opening and with axes oriented randomly with respect to the incident beam has been worked out. This expression leads directly to the expressions derived by Mitra for one- and two-dimensional curved crystallites. For cylindrical shells the peaks are highly asymmetrical. They become sharper and shift towards the higher-angle side as the shell axes become more tilted with respect to the normal to the plane containing the incident and the equatorially diffracted beams. The overall nature of the diffraction pattern remains the same. The effect of increasing the number of scattering centres on each arc is found to be only to increase the peak heights and their sharpnesses. The effect of radial thickness is to cause a peak shift and to give rise to additional peaks. The peak heights are increased and become sharper as the radial thickness increases. The effect of curvature is an increase in the number of peaks, an increase in the general background level of scattering and a decrease in the peak heights.

Introduction

In the course of two previous publications [Mitra (1965) and Mitra & Bhattacherjee (1968) hereafter referred to as I and II respectively], an elementary theory of diffraction by an axially parallel aggregate of curved crystallites has been developed and a general expression for two-dimensional curved crystals has been derived. In the treatment, both the incident and the diffracted beams have been assumed to lie in the same plane as the two-dimensional crystallites. The expression derived is satisfactory in the sense that for the extreme cases of zero curvature and of equiangularly spaced atoms arranged on the circumference of a circle, it leads, as expected, respectively to Bragg's law and to the expression derived by Blackman (1951) for a circular lattice. This expression has also the further property of taking into account the angular opening of the curved crystallites as is the case with the expression derived by Kunze (1956). A further virtue of this expression is that it is a finite series of terms containing Bessel functions of order zero (in contrast with infinite series of Bessel functions of very high order in the expression of the above authors) rendering the task of numerical evaluation comparatively easy. However, it would be more realistic to consider an agglomeration of identical cylindrical crystallites with a given angular opening and with axes oriented randomly with respect to the incident beam – in short, a powder of cylindrical fragments. In this paper, it has been attempted to achieve this.

Derivation of the general expression for diffraction intensity

Each crystallite is considered to be built up of an identical stacking of T identical layers of the type of $ABCD$ [Fig. 1(*a*)], the details being the same as in Fig. 1 of I. The stacking along the Z direction is at equal intervals, c, as shown in Fig. 1(*b*). The curvature lies in the XY plane. $ABCD$ consists of M concentric arcs at radial distances $R, R+b, R+2b, \ldots R+mb, \ldots R+(M-1)b$ respectively. Each arc has N lattice points arranged equiangularly on it so that two consecutive points on the same arc subtend an angle φ at the point of intersection of the axis OZ with the plane $ABCD$. The angular opening is denoted by a parameter Q where $Q=2\pi/N\varphi$. Any lattice point J [Fig.1(*b*)] in the cylindrical lattice occupies the rth site on the mth arc on the tth stack and is described by (r,m,t). The point A is

defined to be (0,0,0) in this system. The vector distance τrmt of J from O, the origin of the system is given by

$$\tau_{rmt} = \mathbf{i}_x(R+mb)\sin r\varphi + \mathbf{i}_y(R+mb)\cos r\varphi + \mathbf{i}_z tc \quad (1)$$

where $\mathbf{i}_x$, $\mathbf{i}_y$, $\mathbf{i}_z$ are unit vectors along the X, Y and Z axes respectively. The vector distance τ_0 of A from O is given by

$$\tau_0 = \mathbf{i}_y R . \quad (2)$$

Let the incident and diffracted beams be described by unit vectors σ_0 and σ respectively with the angle of deviation given by 2θ. Let $\mathbf{s}=\sigma-\sigma_0$ with $|\mathbf{s}|=2\sin\theta$. It is evident that for a fixed value of θ, any rotation of σ_0 will cause a corresponding rotation in $\mathbf{s}$ so that $|\mathbf{s}|$ will remain unchanged. Thus, random orientation of the crystallite with respect to σ_0 is equivalent to randomness in the values of γ and x, where γ is the angle between $\mathbf{s}$ and OZ and χ, the angle made by the projection of $\mathbf{s}$ on the XY plane with OX [see Fig. 2(*b*)].

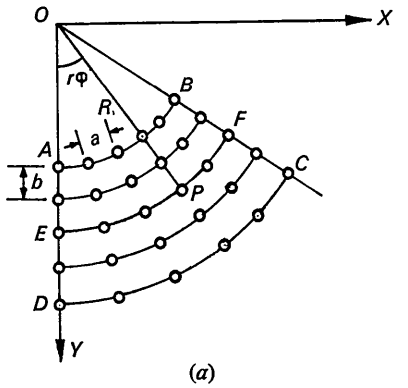

(*a*)

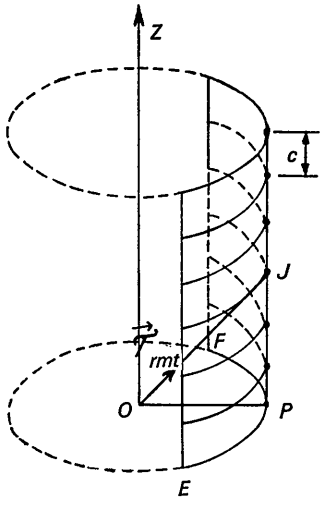

(*b*)

Fig. 1. The cylindrical crystallite with a given angular opening. (*a*) A layer of the bent crystallite in the XY plane. (*b*) Cylindrical shell with axis parallel to OZ. $\vec{\tau}_{rmt}$ denotes the position of a lattice point J from the origin O in the coordinate system XYZ.

Thus

$$\mathbf{s} = \mathbf{i}_x s\sin\gamma\cos x + \mathbf{i}_y s\sin\gamma\sin x + \mathbf{i}_z s\cos\gamma . \quad (3)$$

The amplitude of the beam diffracted along σ will be given by

$$A(\sigma) = \sum_{r,m,t}\sum_{j} f_j(\sigma)\exp i\frac{2\pi}{\lambda}(\tau_{rmt}+\tau_j-\tau_0).(\sigma-\sigma_0) \quad (4)$$

where f_j is the atomic scattering factor of the type j located at distance τ_j from the lattice point (r,m,t). Equation (4) can clearly be written as

$$A(\mathbf{s}) = F(\mathbf{s})H(\mathbf{s})\exp\left(-i\frac{2\pi}{\lambda}\tau_0 . \mathbf{s}\right) \quad (5)$$

with

$$H(\mathbf{s}) = \sum_{r,m,t}\exp\frac{2\pi}{\lambda} i(\tau_{rmt} . \mathbf{s}) \quad (6)$$

and

$$F(\mathbf{s}) = \sum_{j} f_j \exp i\frac{2\pi}{\lambda}(\tau_j . \mathbf{s}) . \quad (7)$$

Obviously the τ_j's have to be consistent with the cylindrical symmetry of the lattice so that equation (4) is transformed into (5). The simplest case is that of a single identical atom occupying each lattice site so that $F(\mathbf{s})=f(\mathbf{s})$ for this case. Combining equations (1) and (3) with (6) we have

$$|H(\mathbf{s})| = \frac{\sin\left(\frac{\pi s}{\lambda}Tc\cos\gamma\right)}{\sin\left(\frac{\pi}{\lambda}sc\cos\gamma\right)}|G(\mathbf{s})| , \quad (8)$$

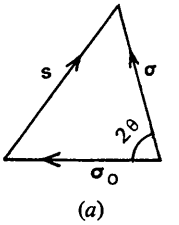

(*a*)

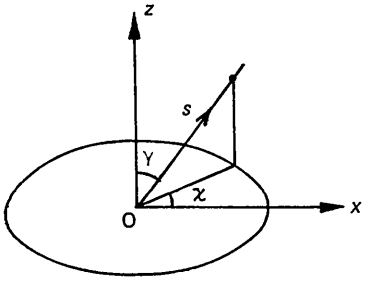

(*b*)

Fig. 2. Orientations of the vector $\mathbf{s}$. (*a*) Direction of vector with respect to the direction of incidence and direction of diffraction. (*b*) Orientation of $\mathbf{s}$ with respect to X, Y and Z axes.

with

$$G(\mathbf{s})=\sum_r \sum_m \exp i\mu(R+mb)\sin(r\varphi+x) \qquad (9)$$

where

$$\mu=\frac{2\pi s}{\lambda}\sin\gamma\,. \qquad (10)$$

The intensity averaged over all values of x is given by

$$I(\mathbf{s})=\langle H(\mathbf{s})H^*(\mathbf{s})\rangle$$

$$=\frac{\sin^2\left(\frac{\pi}{\lambda}sTc\cos\gamma\right)}{\sin^2\left(\frac{\pi}{\lambda}sc\cos\gamma\right)}\,.\,\langle G(\mathbf{s})\,.\,G^*(\mathbf{s})\rangle\,. \qquad (11)$$

It is well known that for $\frac{sc\cos\gamma}{\lambda}=l_0$ (an integer)

$$\frac{\sin^2\left(\frac{\pi}{\lambda}sTc\cos\gamma\right)}{\sin^2\left(\frac{\pi}{\lambda}sc\cos\gamma\right)}=T^2$$

but for other values of l_0 this function is zero for large T and nearly zero for small T.

Thus, for $T\geq 20$ and for an appreciable value of $I(\mathbf{s})$

$$\cos\gamma=\frac{l_0}{l} \qquad (12)$$

where

$$l=\frac{sc}{\lambda}\,. \qquad (13)$$

Equation (9) is of the same form as equation (5) of I. Proceeding as in I, introducing

$$h=\frac{\mathbf{s}.\mathbf{a}}{\lambda}$$

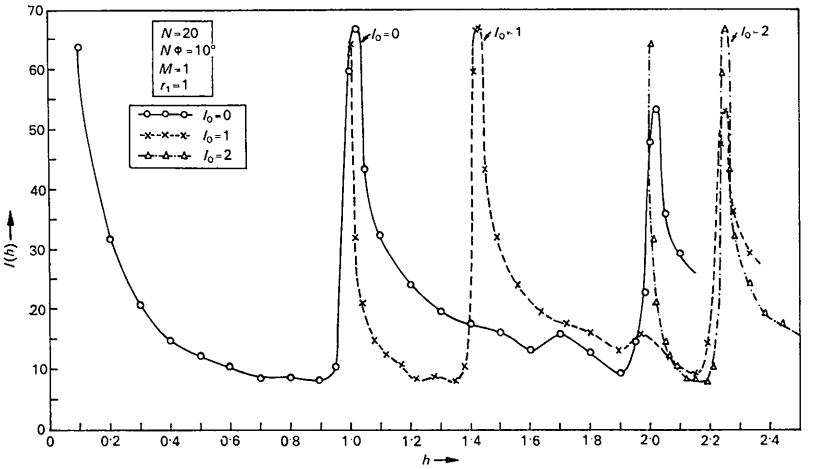

Fig. 3. Relative intensity at different angles of deviation of X-rays diffracted by a random aggregate of identical cylindrical shell fragments with a given angular opening and $r_1=1$ where $r_1=c/a$ and c is the repeat distance in the Z direction.

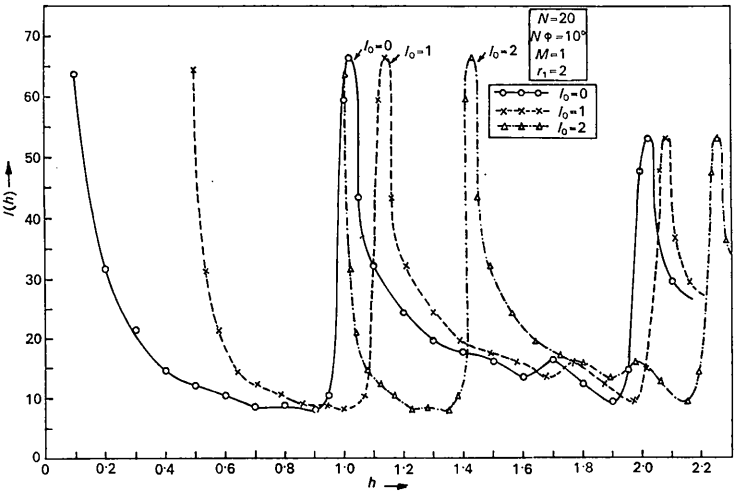

Fig. 4. Relative intensity at different angles of deviation of X-rays diffracted by a random aggregate of identical cylindrical shell fragments with a given angular opening and $r_1=2$ where $r_1=c/a$ and c is the repeat distance in the Z direction.

and

$$k=\frac{\mathbf{s}.\mathbf{b}}{\lambda} \tag{14}$$

and combining with these, equation (13), we can write equation (11) as

$$I(hkl_0)=T^2\sum_{m=0}^{M-1}\sum_{n=0}^{M-1}\sum_{p=-\infty}^{+\infty}J_p\left(QN\{h+mk\varphi\}\sqrt{1-\frac{l_0^2}{l^2}}\right)\times J_p\left(QN\{h+nk\varphi\}\sqrt{1-\frac{l_0^2}{l^2}}\right)\frac{\sin^2 Np\varphi/2}{\sin^2 p\varphi/2} \tag{15}$$

which is identical in form with equation (1) of II. Next proceeding as in II, it is easy to see that equation (15) can be written as

$$I(hkl_0)=T^2\left[\sum_{m=0}^{M-1}\sum_{n=0}^{M-1}NJ_0\left(QNk\varphi\{m-n\}\sqrt{1-\frac{l_0^2}{l^2}}\right)+2\sum_{m=0}^{M-1}\sum_{n=0}^{M-1}\sum_{q=1}^{N-1}(N-q)J_0\left(QN\sqrt{1-\frac{l_0^2}{l^2}}\times\sqrt{\{(h+mk\varphi)^2+(h+nk\varphi)^2-2(h+mk\varphi)\cdot\times(h+nk\varphi)\cos q\varphi\}}\right).\right]$$

or

$$I(hl_0)=T^2\left[\sum_{m=0}^{M-1}\sum_{n=0}^{M-1}NJ_0\left(QNh\varphi\{m-n\}r_2\sqrt{1-\frac{l_0^2}{h^2r_1^2}}\right)+2\sum_{m=0}^{M-1}\sum_{n=0}^{M-1}\sum_{q=1}^{N-1}(N-q)J_0\left(QNh\sqrt{\left(1-\frac{l_0^2}{r_1^2h^2}\right)}\times\left\{(1+mr_2\varphi)^2+(1+nr_2\varphi)^2-2(1+mr_2\varphi)\times(1+nr_2\varphi)\cos q\varphi\right\}^{1/2}\right)\right] \tag{16}$$

where $r_1=c/a$ and $r_2=b/a$ respectively. It is quite obvious that equation (6) of II corresponds to $l_0=0$. For a system comprising axially parallel cylindrical fragments, or for a solitary cylindrical fragment rotating or oscillating about its axis, equation (16) represents the l_0th layer in a layered distribution of intensity. For random orientations of the crystallites, however, all those crystallites which obey equation (12) will be in a position to diffract and the diffraction pattern will have spherical symmetry resulting in Debye–Scherrer rings when photographed. The rings will be sharp or diffuse depending on the parameters in equation (16). The dif-

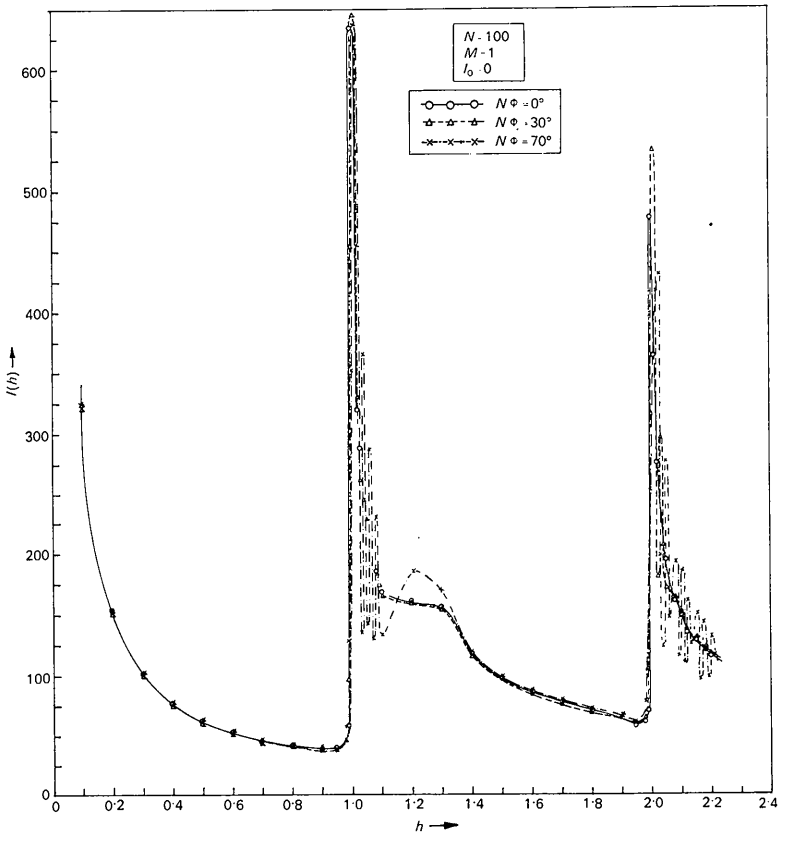

(*a*)

Fig. 5. Relative intensity of X-rays diffracted by an axially parallel ($l_0=0$) aggregate of identical cylindrical shell fragments with (*a*) angular opening $N\varphi=0°$, 30°, 70°,

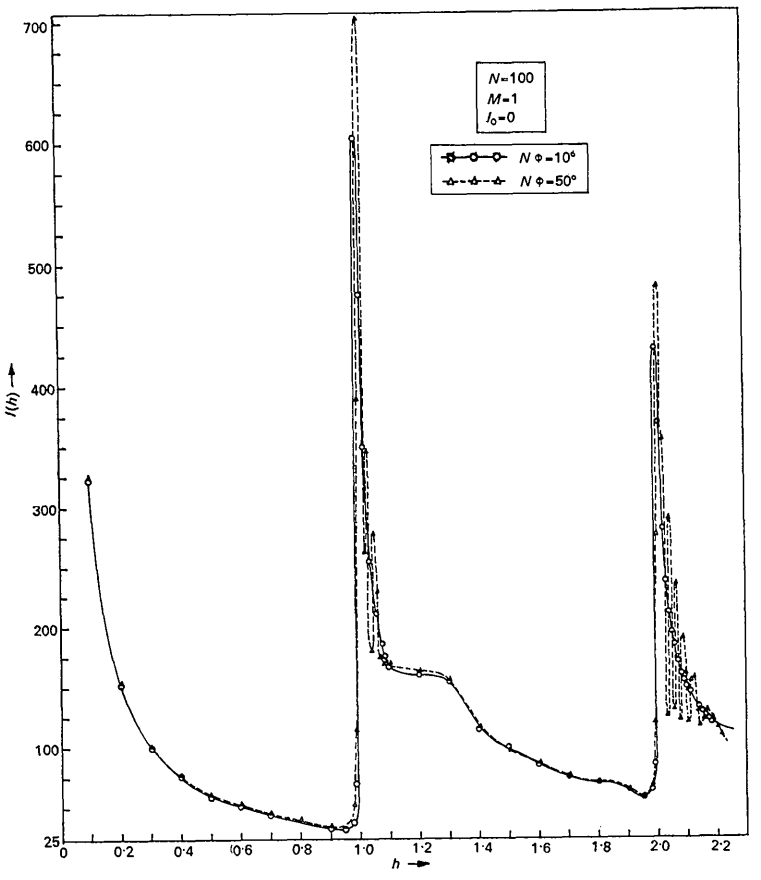

Fig. 5 (*cont.*) (*b*) angular opening = 10°, 50°,

fuse rings may also be bridged by regions of continuous scattering.

The case of a cylindrical shell

For a cylindrical shell, one unit thick in the radial direction $r_2=0$ and equation (16) takes the form

$$I(hl_0)=T^2\left[N+2\sum_{q=1}^{N-1}(N-q)J_0 \times(2QNh\sqrt{1-\frac{l_0^2}{r_1^2h^2}}\sin\frac{q\varphi}{2})\right]. \quad (17)$$

For the case of zero curvature, equation (17) becomes

$$I(hl_0)=T^2\left[N+2\sum_{q=1}^{N-1}(N-q)J_0\left(2\pi qh\sqrt{1-\frac{l_0^2}{r_1^2h^2}}\right)\right]. \quad (18)$$

Equation (17) clearly shows that in the domain $h\geq l_0/r_1$ the effect of $l_0\neq 0$, is merely to shift the diffraction pattern from that due to $l_0=0$ towards a larger value of h given by $\sqrt{h^2+l_0^2/r_1^2}$. When $h<l_0/r_1$, the argument of the Bessel function becomes imaginary and increases as h decreases. As is evident from Figs. 118 and 119 of

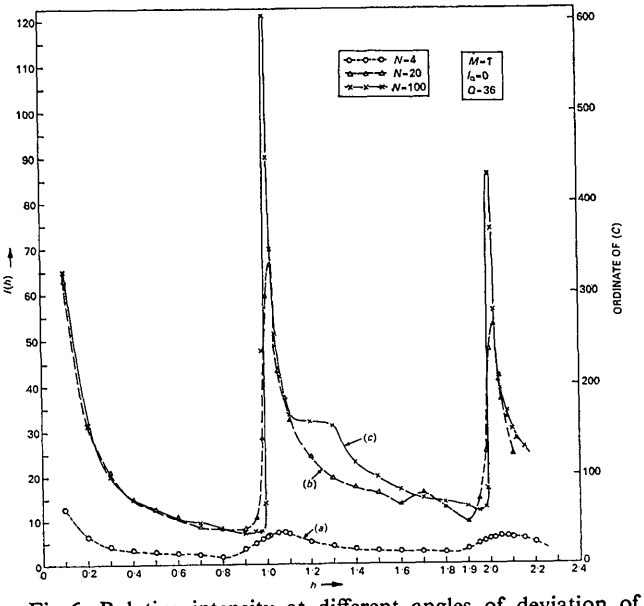

Fig. 6. Relative intensity at different angles of deviation of X-rays diffracted by an agglomeration of axially parallel ($l_0=0$) identical cylindrical shell fragments having $Q=36$ and (*a*) $N=4$, (*b*) $N=20$, (*c*) $N=100$.

Jahnke & Emde (1945), $J_0(ix)$ with x real goes on increasing monotonically with x. Thus, in the domain $h<l_0/r_1$, $I(hl_0)$ of equation (17) will go on increasing monotonically as h approaches zero. Hence all the considerations for a single arc discussed in I and II will be equally valid (except for the form of the peak at $h=0$) in this case also, only with the distribution shifted towards the higher value side of h. It is also clear that when r_1 is small this shift will be larger than when r_1 is large. Hence the interlayer distance c will merely affect the shift. These effects have been shown in Figs. 3 and 4 which show results of calculations for $N=20$, $N\varphi=10°$, $M=1$ and $l_0=0,1,2$ for two different values of r_1 viz. $r_1=1,2$. Fig. 3 which represents $I(h)$ against h for $r_1=1$, shows that the first peak is at $h=1{\cdot}02$ in the case for $l_0=0$ and the corresponding peaks for $l_0=1$ and 2 are found to be at about $h=1{\cdot}43$ and $h=2{\cdot}45$ respectively. Fig. 4 shows that the peak at $h=1{\cdot}02$ for $l_0=0$ shifts to $h=1{\cdot}14$ and $h=1{\cdot}43$ for $l_0=1$ and 2 respectively when $r_1=2$.

Similarly from Fig. 3 it is observed that the second maxima are in the neighbourhood of $h=2{\cdot}02$ and $h=2{\cdot}25$ corresponding to $l_0=0$ and $l_0=1$ respectively. For $l_0=2$ this maximum (not shown in Fig. 3) is found to be formed at $h=2{\cdot}85$. Fig. 4 shows the peak in the neighbourhood of $h=2{\cdot}02$ shifts to $h=2{\cdot}08$ and $h=2{\cdot}25$ corresponding to $l_0=1$ and 2 respectively.

The half intensity widths of the first maxima have been measured from the graphs and in units of h, are

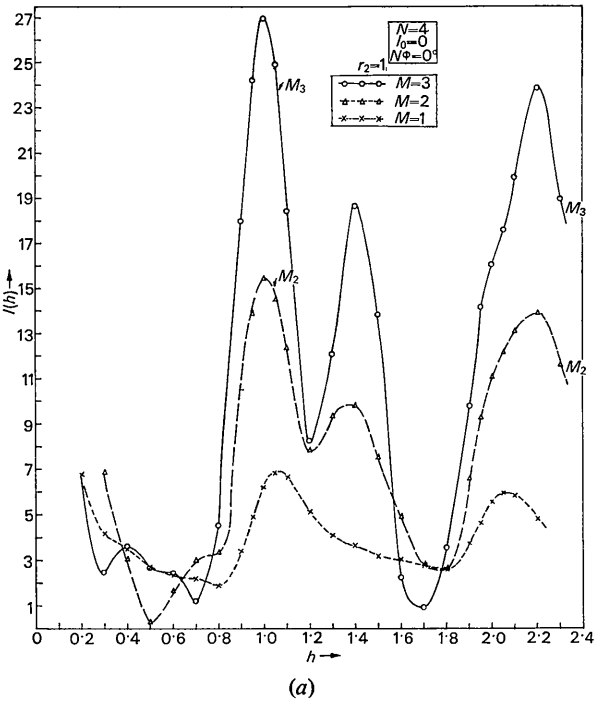

(a)

Fig. 7. Relative intensity at different angles of deviation of X-rays diffracted by an aggregate of axially parallel identical cylindrical crystallites having different radial thickness with $r_2=1$, $N=4$ and (a) $N\varphi=0°$,

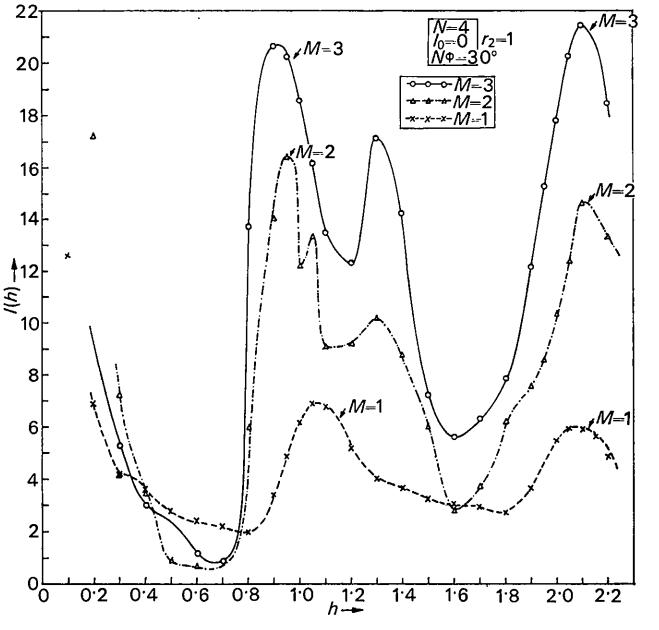

(b)

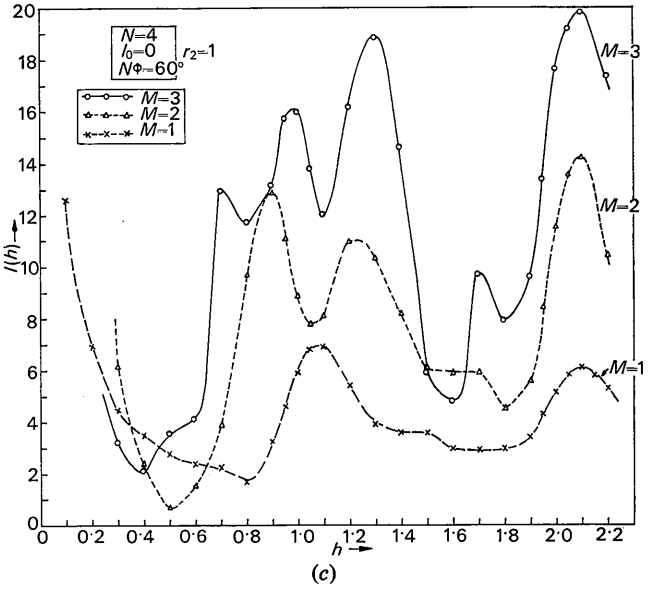

(c)

Fig. 7 (*cont.*) (b) $N\varphi=30°$,(c) $N\varphi=60°$.

equal to 0·085, 0·060, 0·035 (for $r_1=1$) and 0·085, 0·065, 0·050, (for $r_1=2$) corresponding to $l_0=0,1,2$ respectively. Figs. 3 and 4 show further that the peaks are highly asymmetrical.

These observations clearly show that in the case of cylindrical shells, peaks are highly asymmetrical and the asymmetry remains more or less unchanged with the increase in the value of l_0. The peaks, however, become sharper and shift more and more towards the higher angle side as the shell axes become more and mor tilted with respect to the Z axis. The effect of increasing $r_1$is merely to decrease the extent of the shift towards the

higher angle side. But the overall nature of the diffraction pattern remains the same in all the cases.

Effect of curvature

In order to study the effect of curvature on the intensity pattern, calculations were carried out for $N=100$, $M=1$, $l_0=0$, and $N\varphi=0$, 10, 30, 50 and 70° respectively. Fig. 5(*a*) and (*b*) show the results of these calculations. The curves show slight variations in peak positions and heights. The most important feature is the appearance of a number of closely spaced secondary peaks of gradually decreasing heights on the higher angle side of the primary maxima for large values of curvatures ($N\varphi>30°$). The number of secondary maxima is more in the neighbourhood of $h=2$ than $h=1$ for the same value of $N\varphi$. Also their number increases with the increase of curvature. Otherwise the general asymmetrical nature of the distribution remains the same in all cases.

Effect of the number of scatterers on each arc

Numerical computations have been carried out for the case of $M=1$, $l_0=0$, and different values of N for a given value of Q. Fig. 6 shows the results of the computations. Curves (*a*) and (*b*) in Fig. 6 represent $I(h)$ against h for $N=4$ and 20 respectively and $Q=36$ in each case. Curve (*c*), which is plotted in a smaller scale (marked on the ordinate at the right end of the Fig. 6), for the convenience of representation in the same Figure, shows the case for $N=100$ and $Q=36$. It is seen from the curves that the first and second peak for $N=100$ are exactly at $h=1$ and 2 respectively. For $N=20$ and 4 the peak in the neighbourhood of $h=1$ is found to be at $h=1{\cdot}02$ and $1{\cdot}06$ while the second one is at $h=2{\cdot}02$ and $2{\cdot}07$ respectively.

It has been observed in paper II that these peak shifts are a combined and complicated effect of the variation of N and φ. In that paper the effect could not be studied for large values of N. The present work clearly shows that the peak shift is attributable more to the smallness of the number of scatterers than to the curvature. It is seen that even for $N\varphi=70°$ the maximum at $h=1$ shifts to only $h=1{\cdot}01$ [Fig. 5(*a*)] for $N=100$. Hence the peak shift can be attributed mainly to smallness of N and less to the variation of φ. Also it is observed, as is expected, that only the sharpnesses and the peak heights increase with the increase in the number of scatterers on each arc.

Effect of radial thickness

Figs. 7(*a*), (*b*) and (*c*) represent the results of numerical computations for $N=4$; $M=3$, 2, 1; $r_2=1$ and $l_0=0$ corresponding to (*a*) $N\varphi=0°$, (*b*) $N\varphi=30°$, (*c*) $N\varphi=60°$. It is observed from the curves that for the same value of the curvature, the peak shifts towards the higher angle side as the value of M is decreased, while the peak heights and sharpnesses of the peaks increase with the increase in the value of M. Also some additional peaks appear. From these results it appears that the effect of radial thickness is to cause a shift of the peak, and to give rise to additional peaks. The peak heights are increased and become sharper as the radial thickness increases. Also a comparison of Fig. 7(*a*), (*b*), and (*c*) reveals that the effect of curvature in radially thick crystallites is an increase in the number of peaks, an increase in the general background level of scattering and a decrease in the peak heights. It also influences peak shift – the higher the curvature the greater is the peak shift.

The case for zero curvature as shown in Fig. 7(*a*), presents an interesting study. Physically it represents the zero layer rotation pattern of a cubic crystal. h here represents $\sqrt{h^2+k^2}$ for the $hk0$ planes assuming the rotation to be about the (001) axis. Hence $h=1$, $1{\cdot}4$ and $2{\cdot}2$ for (100, 010), (110) and (120) reflexions respectively. As is to be expected, Fig. 7(*a*) shows peaks at these values of h. It is interesting to note that peaks appear in the neighbourhood of the same value of h for curvatures given by $N\varphi=30$ and 60° for the same value of N *viz.* $N=4$. Thus it appears that even as severe a curvature as in the cases discussed does not modify the Laue–Bragg conditions of appearance of diffraction maxima in a radical way. This point, however, needs further and more detailed study which it is proposed to carry out in the near future.

Concluding remarks

The results of these investigations have not taken care of the structure factor $F(\mathbf{s})$. In fact, the actual intensity pattern is the product of $F(\mathbf{s})$ with $H(\mathbf{s})$, the interference term that has been worked out. Hence these results can provide only a qualitative explanation of experimental results. A quantitative comparision with experiments is not possible without complete knowledge of $F(\mathbf{s})$.

References

BLACKMAN, M. (1951). *Proc. Phys. Soc.* B**64**, 631.

JAHNKE, E. & EMDE, F. (1945). *Tables of Functions with Formulae and Curves*, p. 224. New York: Dover.

KUNZE, G. (1956). *Acta Cryst.* **9**, 841, 847.

MITRA, G. B. (1965). *Acta Cryst.* **18**, 464.

MITRA, G. B. & BHATTACHERJEE, S. (1968). *Acta Cryst.* A**24**, 266.